Finding strong lenses in CFHTLS using convolutional neural networks

C. Jacobs[1]⋆, K. Glazebrook[1], T. Collett[2], A. More[3], C. McCarthy[4]

[1]*Centre for Astrophysics and Supercomputing, Swinburne University of Technology, P.O. Box 218, Hawthorn, VIC 3122, Australia*
[2]*Institute of Cosmology and Gravitation, University of Portsmouth, Burnaby Rd, Portsmouth, PO1 3FX, UK*
[3]*Kavli IPMU (WPI), UTIAS, The University of Tokyo, Kashiwa, Chiba 277-8583, Japan*
[4]*School of Software and Electrical Engineering, Swinburne University of Technology, P.O. Box 218, Hawthorn, VIC 3122, Australia*

ABSTRACT

We train and apply convolutional neural networks, a machine learning technique developed to learn from and classify image data, to Canada-France-Hawaii Telescope Legacy Survey (CFHTLS) imaging for the identification of potential strong lensing systems. An ensemble of four convolutional neural networks was trained on images of simulated galaxy-galaxy lenses. The training sets consisted of a total of 62,406 simulated lenses and 64,673 non-lens negative examples generated with two different methodologies. An ensemble of trained networks was applied to all of the 171 square degrees of the CFHTLS wide field image data, identifying 18,861 candidates including 63 known and 139 other potential lens candidates. A second search of 1.4 million early type galaxies selected from the survey catalogue as potential deflectors, identified 2,465 candidates including 117 previously known lens candidates, 29 confirmed lenses/high-quality lens candidates, 266 novel probable or potential lenses and 2097 candidates we classify as false positives. For the catalogue-based search we estimate a completeness of 21-28% with respect to detectable lenses and a purity of 15%, with a false-positive rate of 1 in 671 images tested. We predict a human astronomer reviewing candidates produced by the system would identify ~20 probable lenses and 100 possible lenses per hour in a sample selected by the robot. Convolutional neural networks are therefore a promising tool for use in the search for lenses in current and forthcoming surveys such as the Dark Energy Survey and the Large Synoptic Survey Telescope.

Key words: gravitational lensing: strong – methods: statistical

1 INTRODUCTION

Gravitational lensing is a consequence of the relativistic curvature of spacetime by massive objects such as galaxies, groups and galaxy clusters (Einstein 1936; Zwicky 1937). Since the discovery of the first strongly-lensed quasar by Walsh et al. (1979), the search for and study of strong lenses has become an increasingly active field of astronomy.

Lensing phenomena can tell us much about the characteristics of distant objects and about the universe itself across cosmic time (Wambsganss 1998; Blandford & Narayan 1992; see Treu & Ellis 2015 for an overview). So-called strong lensing occurs where the gravitational potential of a lensing body is sufficient, and the position of a distant source is aligned such that multiple images of the source are produced and are detectable (Schneider et al. 2006; Treu 2010).

Strong lenses have numerous scientific uses including constraining the mass content and density profiles of galaxies for both dark matter and baryons (Treu & Koopmans 2002; Bradač et al.

2002; Treu & Koopmans 2004; Sonnenfeld et al. 2015; Oguri et al. 2014; Auger et al. 2010; Collett et al. 2017) and allowing us to study otherwise undetectable young galaxies at high redshift when magnified by these gravitational telescopes (e.g. Newton et al. 2011; Quider et al. 2009; Zheng et al. 2012).

Strong lenses are also valuable to cosmologists, as they allow allowing us to constrain several cosmological parameters. This includes the Hubble constant and dark energy equation of state, particularly when time delay information is present such as in the case of lensed quasars (Refsdal 1964; Tewes et al. 2013; Suyu et al. 2013; Oguri et al. 2012; Collett & Auger 2014; Bonvin et al. 2016).

Only several hundred high-quality examples of galaxy-galaxy strong lenses are known (Collett 2015, the Masterlens database[1]), but current and next-generation wide surveys are likely to capture many more. Oguri & Marshall (2010) predict some 8000 lensed quasars are to be found in Large Synoptic Survey Telescope (LSST) (Ivezic et al. 2008) imaging and of order 1000 in the Dark Energy

---

⋆ E-mail:colinjacobs@swin.edu.au

[1] Database of confirmed and probable lenses from all sources, curated by the University of Utah. http://admin.masterlens.org

Survey (The DES Collaboration 2005) (DES)[2]. Treu (2010) predicts ~1 lens per square degree with ground-based telescopes and Collett (2015) performed modelling suggesting up to 2400 galaxy-galaxy strong lenses should be identifiable in DES given an optimal stacking strategy, and of order 10^5 should be detectable in the LSST and Euclid (Amiaux et al. 2012) survey databases.

Identifying strong lenses from amongst the many millions of non-lensing galaxies in the surveys of the next decade presents an interesting challenge. Lenses can be complex, spanning a range of morphologies, sizes and colours. Describing them, whether in code or for a human audience, is difficult to do without ambiguity.

With survey databases now in the terabyte-petabyte range, visual search of each potential lens galaxy by a human astronomer is no longer a feasible option, and so we need algorithms to find candidates for us. Previous automation strategies have included searching for features characteristic of strong lenses such as arcs and rings (Lenzen et al. 2004; Alard 2006; Estrada et al. 2007; Seidel & Bartelmann 2007; More et al. 2012; Gavazzi et al. 2014), fitting geometric parameters measuring an arc shape and searching for blue residuals in galaxy-subtracted images.

Marshall et al. (2009) and Brault & Gavazzi (2015) modeled potential lens galaxies candidate as a strong lens system and used the model's fit to the data as an estimate lens candidate likelihood.

Other approaches include using principal component analysis to subtract galaxies from imaging data (Joseph et al. 2014); parameterising the colour and shape of lensed quasars (Chan et al. 2015); and training thousands of citizen scientists on simulated images and then having them visually inspect cutouts (Marshall et al. 2016; More et al. 2016, hereafter SWI and II).

Each methodology has successfully identified tens to hundreds of new lenses or high-quality candidates for follow-up (e.g.~59 in SWII). The problem faced by any automated strategy is the wide variety of morphologies present in strong lens systems and the potential for confusion with non-lenses, such as blue spiral galaxies. The difficulty in paramaterising the full range of potential lenses has meant that inspection by human experts has remained both a cornerstone and bottleneck in lens-finding efforts.

In contrast to traditional approaches, machine learning classification techniques forego human intuitions regarding the weighting and relationships of significant features of the dataset and instead algorithmically extract a useful parameterisation from patterns present in the data only (see Jordan & Mitchell 2015 for a brief overview of current machine learning applications). The application of machine learning techniques to 'big data' challenges in astronomy is an active field of research at present. Artificial Neural Networks (ANNs) in particular have been successfully applied to astronomical problems. Dieleman et al. (2015) used convolutional neural networks to replicate human judgements about Sloan Digital Sky Survey (SDSS) galaxy morphology as part of a GalaxyZoo Kaggle challenge[3] and Huertas-Company et al. (2015) applied them to morphological classification in the CANDELS fields. Hoyle (2016) used deep learning (see Section 2) techniques for photometric redshift estimation. Schawinski et al. (2017) employed Generative Adversarial networks (Goodfellow et al. 2014) to develop a novel deconvolution technique and recover features in SDSS galaxy images. In the lens-finding arena, Bom et al. (2017) employed neural networks and the Mediatrix Filamentation

Method, while Ostrovski et al. (2017) applied Gaussian Mixture Models to the lensed quasar search.

The success of these machine learning techniques in other areas of astronomy, and more broadly in computer vision (i.e. the identification and classification of objects in digital images) makes them a promising candidate for learning and detecting the particular morphology of strong lenses. However, inherent in all supervised learning methodologies, especially in convolutional neural networks, is the need for a large, diverse and fully-labelled training set with which to tune the network's weights. Training sets for complex image classification networks are typically of the order of 10^6 images and anything smaller than 10^4 images is unlikely to suffice for robust training of a complex network which may have order 10^7 to 10^9 parameters to be optimized. The work is further complicated by the rarity of strong lensing systems, with the implication that any sub-optimal classifier will overwhelm good potential lenses with false positives.

In this work we develop the application of convolutional neural networks to detecting the morphology of galaxy-galaxy lenses in optical images. We focus on developing a synthetic training set of sufficient size and quality, and on ensuring that false positives were minimised. We use the lens quality grade scale as outlined in SWII, with images 0) unlikely to contain a lens, 1) possibly containing a lens, 2) probably containing a lens and 3) almost certainly containing a lens. In this paper we define false positives as any candidates that we judge to be grade 0.
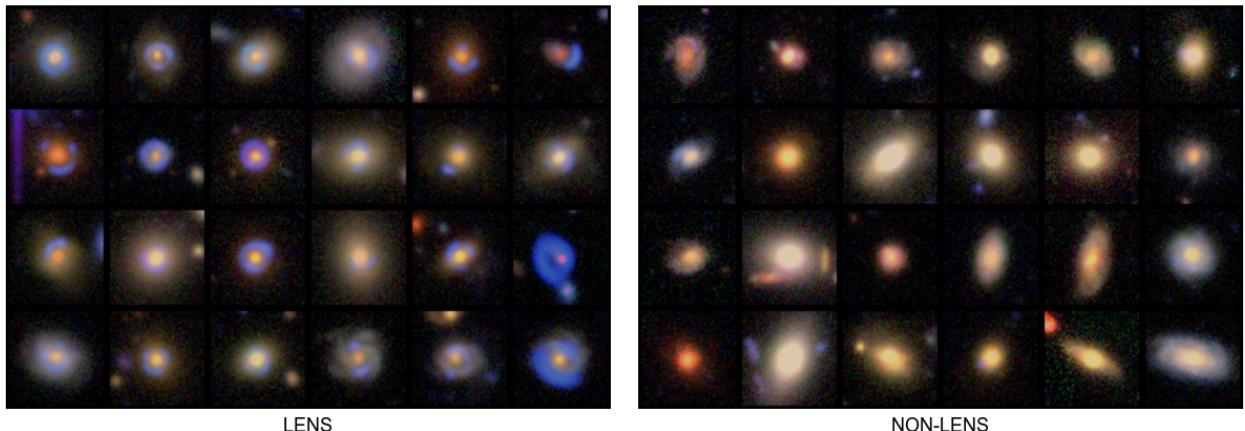
The Canada France Hawaii Telescope Legacy Survey (CFHTLS) was chosen for our search as it has been extensively searched for strong lenses previously, providing us with an opportunity to benchmark the performance of this approach. As well as visual searches (Elyiv et al. 2013; Sygnet et al. 2010) and serendipitous discoveries (Thanjavur 2009) there have been several previous robotic searches of the entire survey as part of the CFHTLS Strong Lensing Legacy Survey (SL2S) (Cabanac et al. 2007). More et al. (2012) used the ARCFINDER robot and Gavazzi et al. (2014) used the RINGFINDER algorithm to detect galaxy and cluster-scale strong lenses. These two searches, in addition the SPACEWARPS search, have collectively identified over 500 lenses and potential lenses which we can use to assess the effectiveness of our own algorithm. These searches and the lenses they discovered are detailed in Section 2.2.

In this paper we present our convolutional neural network-based lens finder and apply it to the CFHTLS survey. The paper is organised as follows: Section 2 provides a brief overview of artificial neural networks and the training process that powers them, and details the results of previous automated lens searches in the survey. In Section 3 we describe the challenges of lens finding and how we assemble our networks and the simulated lens training sets to train them, as well as the two strategies we employ in their application to the survey data. In Section 4 we apply our lens finder to 171 square degrees of the CFHTLS survey and describe the lens candidates we recover, including known, confirmed lenses and novel candidates. In Section 5 we examine the limitations of the two survey search approaches, the use of ensembles of neural networks, and how best to quantify the performance of the robot. Finally, in Section 6 we summarise the performance of our lens finder and provide a brief outlook of how future work may improve its performance and usefulness to astronomy.

---

[2] http://www.darkenergysurvey.org
[3] https://www.kaggle.com/c/galaxy-zoo-the-galaxy-challenge

Training set 1 (SIMCT)

LENS   NON-LENS

Training set 2 (LensPop)
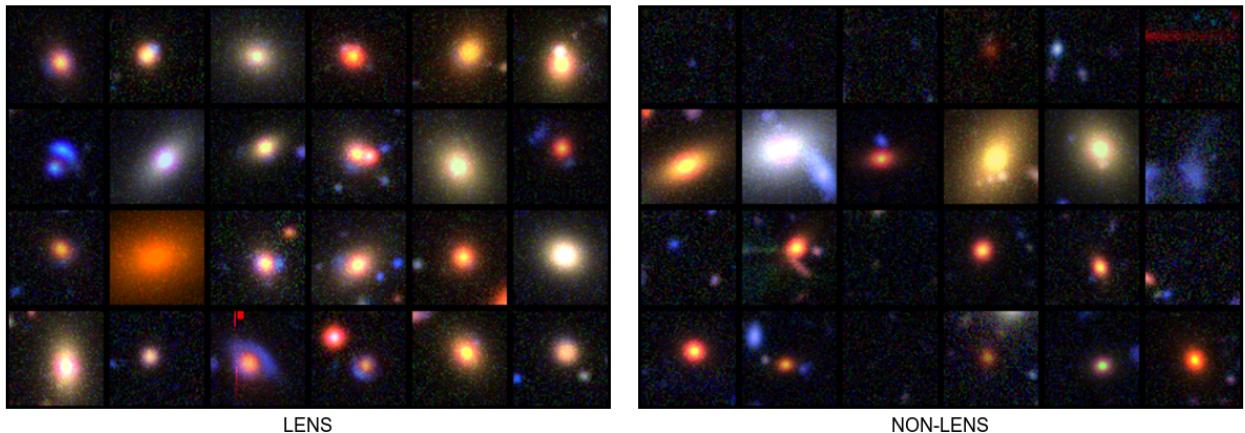

LENS   NON-LENS

Figure 1. Example synthetic lens images from two training sets. Top: synthetic lensed sources on real survey galaxies. Bottom: Synthetic source and deflector, on real survey backgrounds.

2 BACKGROUND

Artificial Neural Networks (ANNs) were first described as far back as the 1950s (Rosenblatt 1957) and were refined over decades, but fell into relative disuse in favour of other algorithms due to performance and scaling issues. More recent advances in the algorithms, including improved network initalisation (Hinton & Salakhutdinov 2006), optimized gradient descent methods (Duchi et al. 2011; Zeiler 2012), dropout (Hinton et al. 2012), as well as improvements in hardware and the availability of large labelled data sets, have enabled "deep learning" - training ANNs with many layers - and a resurgence in their use. In recent years the field of computer vision has been revolutionized by advancements in deep learning techniques, in particular the use of convolutional neural networks ("ConvNets" - Fukushima (1980); Lecun et al. (1998)). In 2012 Krizhevsky et al. (2012), employing a convolutional neural network of novel design, entered the benchmark ImageNet Large-Scale Vi-

sual Recognition Challenge[4] (ILSVRC - Russakovsky et al. 2015) and were able to surpass in accuracy the state-of-the-art of conventional computer vision techniques by 10%, an impressive margin. Since then, the development and application of convolutional neural networks remains an active area of research (Zeiler & Fergus 2014; Szegedy et al. 2014; Simonyan & Zisserman 2014; He et al. 2015).

Artificial neural networks, named by analogy to the neuronal network in the brain that inspired their design, are constructed as a layered network of interconnected nodes ("neurons"), each of which takes a weighted vector as inputs and outputs a scalar value passed through an activation function - a differentiable function that introduces non-linearity into the network. At the first layer, the raw inputs are weighted and passed as inputs to a layer of input neurons. This is repeated for an arbitrary number of intermediate "hidden" layers. At the last layer, the outputs are interpreted as an approx-

---

[4] An annual competition considered the benchmark in computer vision performance, with a training set of 10^6 images across 1000 categories. http://www.image-net.org/challenges/LSVRC/

imation function appropriate to the problem domain, such as the probability that the input is member of a particular class. For a network of sufficient size and complexity, arbitrary logic can be represented in the connections between artificial neurons, encapsulated by the weights that parameterise the network.

Convolutional neural networks extend ANNs by taking advantage of the spatial relationship between input values, namely, the pixels in an image. In a convolution layer, instead of fully connecting all neurons, groups of input neurons are applied to small regions of neighbouring pixels, and the associated weights are shared amongst many groups. This approach has several desirable properties. It vastly reduces the number of weights that characterise the network, and exploits key characteristics of the visual domain such as the spatial significance of neighbouring pixels and translational invariance. These small groups of weights (kernels) are convolved with the image and act as feature detectors. At earlier layers they perform the function of detecting simple geometric features such as edges or patches of colour; at later levels the hierarchy of features becomes increasingly abstract. In standard computer vision applications such as everyday object classification, a network may first activate on patterns such as curves and corners; then features that resemble more complex shapes such as wheels and doors; and finally recognise the arrangement of these features as a truck.

Strong Lenses too have a particular and distinctive morphology, information which must be used by any automated lensfinder (at least in the absence of quality spectroscopic data). For this reason we test the most successful computer vision technique developed to date. We explore whether the algorithm can develop a similar feature hierarchy that is useful in the astronomical context of strong lens finding.

In assessing the quality of a sample produced by a network, the astronomical terminology of purity and completeness differ in their definitions slightly from the terms used in the computer science literature. In this work we use these conventional astronomical terms where possible. A definition of these terms, and others used to describe the performance of the classifier, is presented in Table 1.

2.1 Training Neural Networks

The essence of machine learning techniques is the algorithmic extraction of patterns from data. Supervised learning techniques, such as that presented here, take a labelled (i.e. pre-classified) data set and use it to iteratively optimize a function that parameterizes the differences between the classes of data presented. The training of ANNs involves the optimization of a loss function using the techniques of backpropagation (Hecht-Nielsen 1989) and stochastic gradient descent (Bottou 2010). In brief: mathematically we consider our neural network as a large differentiable function that is parameterized by a set of weights $\mathbf{W}$ which, for any input vector $\mathbf{x}$, outputs a vector $\mathbf{y} \in \mathbb{R}^N$ which we interpret as the probabilities that $\mathbf{x}$ is a member of a defined set of N categories:

$$\mathbf{y} = F(\mathbf{x}, \mathbf{W}) \tag{1}$$

We then take a training set $\hat{\mathbf{X}}$ consisting of of k examples, together with labels of known correct categories $\hat{\mathbf{y}}$. We define a loss function L:

$$L = L(\mathbf{y}, \hat{\mathbf{y}}) \text{ where } \hat{\mathbf{y}} = F(\hat{\mathbf{X}}, \mathbf{W}) \tag{2}$$

such that $L \approx 0$ if $\mathbf{y} = \hat{\mathbf{y}}$ (all examples classified correctly with probability 1) and L increases as the number of mis-classifications on the training set increases. A cross entropy loss function per Cao et al. (2007) is a conventional choice. The problem then becomes

to minimize the function L by finding the optimum set of weights $\mathbf{W}$ given our training set $\hat{\mathbf{X}}$. We do this using a gradient descent method, iteratively calculating the gradients $\frac{\partial L}{\partial W_i}$ for each $\mathbf{x}$ in $\hat{\mathbf{X}}$ and W_i in $\mathbf{W}$, updating $\mathbf{W}$ accordingly until we converge to a minimum value of L. The back-propagation algorithm for calculating the weight gradients and the stochastic gradient descent method used to minimize L and converge on a set of weights are described fully in LeCun et al. (1989).

2.2 Known lenses and candidates

Previous systematic searches of the CFHTLS data have yielded over 500 potential lens candidates. The CFHTLS Strong Lensing Legacy Survey (SL2S) (Cabanac et al. 2007; More et al. 2012; Gavazzi et al. 2014; Sonnenfeld et al. 2013) employed several methods to identify strong lenses in the CFHTLS imaging. More et al. (2012) used the ARCFINDER (Seidel & Bartelmann 2007) algorithm, visually inspecting 1000 candidates per square degree, and yielding a final sample of 127 high-quality candidates. From Sonnenfeld et al. (2013) we include 13 further SL2S lenses confirmed with spectroscopic follow-up. Gavazzi et al. (2014), using the RINGFINDER robot, report a purity and completeness of 42% and 29% (86% and 25% after visual inspection) on simulations, and present 330 good quality (grade > 2) candidates from visual inspection of a sample of 2500 (13%) returned by the algorithm on CFHTLS imaging data. In addition, we include 55 candidates listed from earlier versions of RINGFINDER and other searches that were not included in the other papers. Of these SL2S candidates, 104 have follow-up indicating definite or probable lens status.

We also include 59 new candidates identified in SWII of grades 1-3, as discovered by 37,000 citizen scientists of the SPACE-WARPS program. These lenses form a test set we use for optimising search parameters as outlined below in Section 2.3.

We found 13 other confirmed lenses lying within the CFHTLS footprint had been discovered serendipitously in Hubble Space Telescope (HST) images, and two in SDSS spectroscopic data. These lenses are not detectable in CFHTLS images and so we do not include them in the analysis.

Table 2 depicts the catalogue we assembled after removing duplicates and several lenses for which we did not have imaging available.

2.3 Assembling a test set

We use the 59 lens candidates discovered by the SPACEWARPS citizen scientists as a test set to aid in evaluating and optimising the performance of our robot. The test set consists of candidates of a high quality, which were not used in training the robot, nor are they counted in determining the final performance metric of confirmed CFHTLS lenses recovered. Besides the size and quality of this set, we chose to use the SWII lenses as a test set since, firstly, the lenses were of a size and morphology that made finding by automated means challenging (they were not discovered in any previous CFHTLS lens search); and secondly, they allow for a comparison, in terms of efficiency of search time, with the person-hours invested in training and searching by the SPACEWARPS volunteers who discovered them.

Table 1. Comparison of terminology in machine learning and astronomy as applied to sets of candidate objects.

Astronomical term	Machine learning term
Purity: The fraction of the returned sample that consists of genuine examples of the objects studied. **Completeness**: The fraction of the genuine objects studied that are included in the returned sample.	**Precision**: The fraction of the examples identified by the machine learning algorithm that are true positives. $\frac{TP}{TP+FP}$ **Recall**: The fraction of the positive examples identified by the machine learning algorithm ($\equiv$ **True Positive Rate**): $\frac{TP}{TP+FN}$ **False Positive Rate**: The fraction of negative examples classified incorrectly by the machine learning algorithm: $\frac{FP}{FP+TN}$ **Accuracy**: The fraction of examples classified correctly by the machine learning algorithm: $\frac{TP+TN}{totalsize}$

Table 2. The lenses and potential lenses within the CFHTLS survey reported in previous searches which we use as a benchmark to measure lens-finder performance. Those with reported spectroscopic or imaging follow-up (as compiled by the Masterlens database) we consider confirmed.

Source	Candidates	Confirmed
SL2S More+12	117	57
SL2S Sonnenfeld+13	13	13
SL2S Gavazzi+14	376	34
More+16	59	0
Total	565	104

Table 3. Details of the four Convnets applied to the search. ConvNet1 and ConvNet2 were trained for the all-survey search, then two networks with an extra convolutional layer and training sets tailored for the catalogue-based search were trained. All four networks were applied to the catalogue-based search.

Network	Training set	Architecture	Ensemble
ConvNet1	TS 1	ARCH1	All-survey, catalogue
ConvNet2	TS 2	ARCH1	All-survey, catalogue
ConvNet3	TS 3	ARCH2	Catalogue
ConvNet4	TS 4	ARCH2	Catalogue

3   METHOD

Constructing our lens-finding robot and using it to identify candidates in the survey involves the following steps. Firstly, we construct several training sets of simulated lenses and non-lenses. We also assemble a test set of real survey images containing the 59 SWII lenses/candidates. We use the simulated images to train two convolutional neural networks of our own design using the Caffe open source deep learning framework (Jia et al. 2014), and evaluate their performance on the test set. Counting the number of lenses recovered and the false positives identified in the test set allows us to optimise several parameters for use in a wider search of the entire survey image dataset ("all-survey search"). We then evaluate 6.4×10^8 postage stamps from the CFHTLS survey with each of the two trained networks to produce a candidate set for grading by visual inspection. Subsequently, we adjust the training set and network architecture and train two further neural networks, and use an ensemble of all four of our networks in a more restricted search of images of potential lensing galaxies chosen using a colour-magnitude cut from the survey catalogue. The networks, training sets and architectures used are summarised in Table 3.

3.1   Training Data

In order to apply convolutional neural networks to the lens-finding problem, we must first assemble a training set to optimise the network. The number of known galaxy-galaxy strong lenses is of order 10^2, which practice suggests is several orders of magnitude below the minimum required to usefully train a ConvNet. Furthermore, images of known lenses stem from a heterogeneous mix of surveys, instruments and bands. We must employ an alternate strategy to assemble a training set of appropriate size and consistency. Fortunately, gravitational lensing can be readily modelled using basic physical principles. Here we take the approach of generating synthetic data - simulated lenses in sufficient quantity to form a practical training set.

We assume that, if the artificial lenses are realistic enough, then the network will learn lensing features, such as colour and geometry, sufficiently well to generalize successfully to real astronomical data. Conversely, any errors or biases in the training set are likely to be reflected in the ConvNet's performance, not necessarily in predictable ways. For lens finding, we require that the lensing galaxies and sources should match the colour, size and shape distributions of the real universe as closely as possible; the training set should be adapted for the seeing and filters of the particular target survey, in this case CFHTLS; noise (shot and sky) should match the realistic values for the integration times present in the survey imaging.

Free parameters include the number of examples, the format and dimensions of each training image, the location of lenses in the images and the composition of the negative examples (i.e. non-lens training images).

We employ two strategies to assemble training images conforming to the above constraints. The first strategy involves identifying potential deflector galaxies in the survey, and adding a simulated lensed source galaxy to the survey image. This method is implemented in the SIMCT[5] pipeline described in detail in SWII but can be summarized as follows. Potential deflector galaxies, primarily large, massive early-type galaxies (ETGs), are selected from the CFHTLS catalogue by brightness, colour and photometric redshift. A model mass distribution is assigned to each galaxy using a singular isothermal ellipsoid profile and aligned with the image. Artificial sources are constructed according to the observed parameters of redshift, luminosity and size and given plausible surface brightness profiles and ellipticities. The multiple images of the source are then generated and added to the deflector image using GRAVLENS (Keeton 2001) raytracing code with noise and seeing simulated to match those present in the CFHTLS. As the number of synthetic lens examples is limited to the lens candidate catalogue, the data

---

[5] https://github.com/anupreeta27/SIMCT

is augmented by applying three 90 degree rotations and a random translation of ± 10 pixels in each axis to create four training images per catalogue galaxy.

Our second strategy for generating a training set is to generate mock images where both the lens and source are simulated. This has the advantage that the number of examples that can be generated is effectively infinite, but has the disadvantage that noise, seeing and artifacts must also be simulated to well match real survey data. We do this using a modified version of the LENSPOP[6] code (Collett 2015). LENSPOP uses the observed velocity dispersion function of elliptical galaxies (Choi et al. 2007) to generate a population of singular isothermal ellipsoid (SIE) lenses, with realistic mass, redshift and ellipticity distributions. Lens light is then added using the fundamental plane relation (Hyde & Bernardi 2009) assuming a de Vaucoulours Profile and the spectral energy distribution of an old, passive galaxy. Sources are assumed to have an elliptical exponential profile, with redshifts, sizes and colours drawn from the simulated faint source catalogue of Connolly et al. (2010).

In principle LENSPOP can simulate lenses with extremely faint arcs or extremely small Einstein Radii. In practice such systems are undetectable as lenses and will not contain sufficiently strong features to usefully train the ConvNets. We therefore adopt the detectability criteria defined in (Collett 2015), with a signal-to-noise ratio >20, magnification of 3 or greater and a resolution threshold calibrated such that arcs and counter-images can be resolved from each other and the lens. Only these detectable lenses are used to form our training set.

We modified LENSPOP to generate mock images with appropriate seeing (0.8" in all bands) and shot noise for the CFHTLS, but without readnoise or shot noise from the sky background. These mock images were then superimposed on backgrounds chosen randomly from a tile of the CFHTLS survey. Non lenses were generated in the same way but with the source fluxes set to zero; this results in images with synthetic early-type galaxies drawn from the same distribution as our lenses but with no source light.

The redshift distributions of the simulated lenses and sources are as per Collett (2015) and SWII.

For the whole-survey search, where every pixel of the image database was tested, the ConvNets are required to distinguish strong lensing systems from any other object visible in the survey sky. In the case of the first training set, negative examples consist of images centered on an assortment of galaxies (ellipticals, spirals and irregulars) with no lensed source (Figure 1). For the second training set, we test a different strategy, with negative examples containing empty sky, spiral galaxies, stars, and artifacts, drawn from a random position on a survey tile as 60x60 pixel stamps from the survey imaging.[7] The two training sets (TS1 and TS2) are outlined in Table 4. 20% of the images in each training set are excluded from training and set aside as validation sets for measuring accuracy during the training process.

For the catalogue-based search, all tested images are postage stamps of pre-selected red elliptical galaxies and so the training sets are constructed accordingly. Two further training sets are constructed. The first (TS3) uses SIMCT simulated lenses with a small random translation of 0-10 pixels. The negative training set con-

Table 4. Summary of the image sets used to train the corresponding convolutional neural networks. SIMCT simulations use real survey ETGs and simulated sources; LensPop simulates both source and deflector.

Training set	Simulations	Pos examples	Neg examples	Total
TS1	SIMCT	6657	7813	14470
TS2	LENSPOP	11799	12910	24709
TS3	SIMCT	3950	3950	7900
TS4	LENSPOP	40000	40000	80000

sists of an equal number of ETGs randomly selected from our catalogue. The second (TS4) consists of 40,000 LENSPOP-simulated lenses, again with up to 10-pixel scatter from the centre of the image, and an equal number of catalogue ETGs as the negative training set (unlike TS2, which included stars, empty sky, etc. in the negative set). The spatial jitter, added to TS3 and TS4, is introduced in order to prevent the ConvNets from developing an over-sensitivity to position in the image.

Determining the optimal size of a training set is not straightforward, as it depends on the number of weights to be trained and the complexity of the features the network must learn. Large-scale visual recognition applications typically require training sets in the millions. We assume that, given the small number of convolutional layers (as outlined below) and classes (two) that a training set of order a few times 10^4 to 10^5 examples will suffice to train our networks.

3.2 Network Architecture and Pipeline

The convolutional neural networks were trained using the Berkeley Caffe deep learning package. Two network architectures are used, the first (ARCH1) consisting of two convolutional layers and two fully connected layers of 4096 neurons each, the second (ARCH2) consisting of three convolutional layers and two fully-connected layers of 1024 neurons each (Figure 2). These networks with two to three convolutional layers can be compared to the five of the ILSVRC Alexnet (Krizhevsky et al. 2012) and up to hundreds in the more recent literature (e.g. Simonyan & Zisserman 2014). A smaller network requires less time to train, and our architecture is justified by the smaller and morphologically simpler dataset as well as the low number of categories - two - compared to more general computer vision applications (c.f. ILSVRC, 10^6 images, 1000 categories). ARCH2 added a convolutional layer and reduced the number of fully connected neurons; this design resulted in a smaller number of weights to train (1.1×10^6, versus 1.8×10^7 in ARCH1). Between each layer we use a rectified linear unit ("ReLu") activation function (Nair & Hinton 2010), $y = \max(0, x)$.

The output of each ConvNet was a softmax layer[8] resulting in a real-valued number $0 \leq s \leq 1$ which we interpret as the network's confidence that the candidate image is a lens.

The networks are trained with input images of dimension 60x60 pixels in three colours. These dimensions are chosen as, in the case of CFHTLS imaging at .186" per pixel, this is large enough to contain the test set lenses and small enough to prove highly performant in training and searching. The FITS images in three bands

---

[6] https://github.com/tcollett/LensPop
[7] Since the negative examples were chosen at random from the survey images there is a chance that a few lens candidates could be included. Since their effect on the network is in proportion to their number in the training set, this is unlikely to be a significant problem.

[8] A normalised exponential function that squashes an array of N real values to a N-dimensional vector $\mathbf{v}$ such that $0 < v_i < 1$ and $\sum(v_i) = 1$: $\sigma(z)_j = \frac{e^{z_j}}{\sum_{n=1}^{N} e^{z_n}}$ for $j = 1, ..., n$.
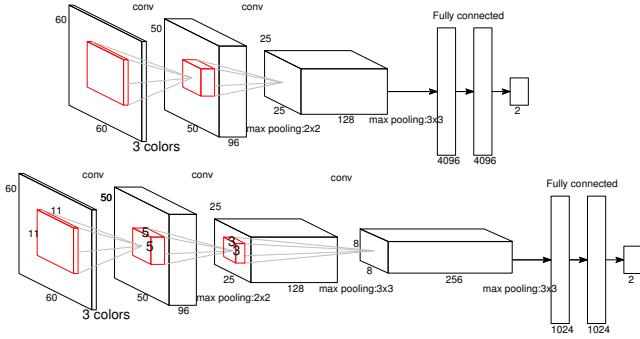
Figure 2. Convolutional network architectures. The networks consist of a) two convolutional layers with kernel sizes 11x11 and 5x5, with 96 and 128 feature maps respectively (ARCH1); and b) three convolutional layers with kernel sizes 11x11, 5x5 and 3x3 with 96, 128 and 256 feature maps (ARCH2). Between each layer is a ReLu activation layer and dropout of 0.5 is applied before each fully connected layer.

are converted to RGB images scaled with an arcsinh stretch using HUMVI (Marshall et al. 2015) and supplied to the ConvNet as vectors of 10800 (60x60x3) floating-point numbers. Due to the optimal depth and quality of CFHTLS *irg*-band images we choose these bands for all images generated for this study, consistent with SWII images seen by volunteers.[9]

Training, when performed on a single NVidia K80 GPU, was typically of order a few hours for ten epochs (iterations through the entire entire training set). Training was conducted using stochastic gradient descent, with Nesterov momentum of 0.9 and a decaying learning rate initialised at 0.1. The network's weights were initialized according to the Xavier method (Glorot & Bengio 2010).

3.3 All-survey search

Two networks of the same architecture (ARCH1) are trained separately on the first two training sets outlined in Section 3.1 and Table 3. As discussed below, an ensemble of the two is used in identifying final candidate lenses. Our processing pipeline constructs the set C of candidate lenses such that for any image c with ConvNet scores s_1 and s_2:

$$c \in C \text{ if } s_1(c) > t_1 \text{ and } s_2(c) > t_2 \qquad (3)$$

where thresholds t_1 and t_2 are parameters chosen empirically to achieve an optimal balance between purity and completeness. As described below, the results presented here assume $t_1 = t_2 = 0.95$.

When processing each pointing image of 19354 pixels squared, our pipeline divides the image into overlapping 60x60 cutouts (in three colours) advanced with a 10-pixel stride, so that any given point in the field will be tested at different positions in 36 cutouts. This means that for each square degree of sky in the survey, 3.7 million overlapping images are tested with each of the two trained ConvNets.

We filter the candidates that meet this criterion further by removing those that are not robust under small translations. We find that rejecting candidates that occurred in isolation, with no neighbouring candidates in overlapping images, removed 85% of candidates and reduced the false positive rate accordingly.

---

[9] See Terapix T0007 release explanatory document: http://terapix.iap.fr/cplt/doc/T0007/doc/T0007-doc.pdf
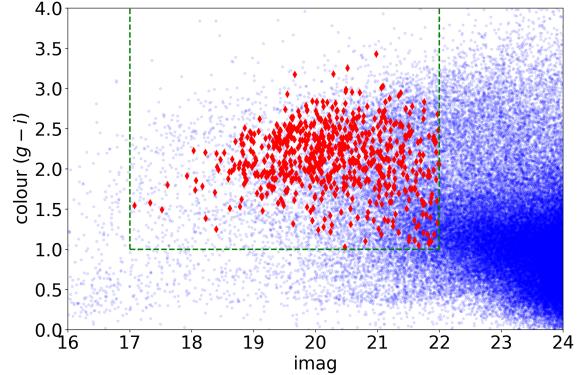
Figure 3. Colours and magnitude of sources from the CFHTLS photometric catalogue (blue dots) and sources corresponding to lensing systems and promising candidates reported in the literature (red diamonds). Our search considers only sources within the box marked in the green dashed line, where ($17 < \text{mag}_i < 22$) and ($g - i > 1$) representing 1.4 million of the 36 million catalogued sources.

3.4 Catalogue-based search

For the catalogue-based search, we restrict the search to catalogued sources in a subset of colour-magnitude space consistent with likely lensing galaxies. We expect massive ETGs to be the best candidate deflectors due to their higher lensing potential, and so select sources that are both bright ($17 < \text{mag}_i < 22$) and red ($g - i > 1$). These thresholds are confirmed by examining the position in colour-magnitude space of known lensing systems and candidates within the CFHTLS footprint (see Figure 3) according to the 3" aperture photometry available in the survey catalogue. 98% of these lenses are within the cut, which contains 5.6% of the 36 million catalogue sources. We apply these cuts to the CFHTLS catalogue, excluding those sources flagged as stars, to build our catalogue of 1,402,222 sources.

For each source in the catalogue, 60x60 pixel postage stamps centered on the source are created and scored by each of the four ConvNets.

4 RESULTS

4.1 Simulated Lenses

All of the networks trained were able to distinguish simulated lenses from non-lenses with high accuracy. On test sets not used for training, containing equal numbers of simulated lenses and non-lenses, the four networks trained were able achieve accuracy of 98.4%, 91.6%, 99.2%, and 99.8%, respectively. This performance is depicted in Figure 4. On test sets of 2000 simulated lenses, the four networks achieved both high purity (94%, 94%, 100%, 100%) and completeness (96%, 95%, 99%, 100%) with a score threshold of 0.5.

The networks' performance dropped when applied to simulated lenses generated by the method not used for training, indicating a preference for the peculiarities of each particular simulation method. Figure 4 depicts the degraded performance for networks 3 and 4 on each other's test sets. However, both the mean and maximum scores of the two networks were able to classify the combined test set with close to 100% accuracy. This fact informed the use of

a combination of the two types of networks on the search of real survey images as outlined below.

4.2   All-survey search

Two ConvNets (ConvNet1 and ConvNet2) were trained on the training sets (described above in Section 3.1) and applied to a test set consisting of 59 512x512 pixel images centered on the lens candidates from SWII. The area covered by the test set is ~3900 pixels squared, equivalent to 0.041 square degrees of sky, which results in a total of 153,459 overlapping 60x60 cutouts to be tested. The parameters t_1 and t_2 from Equation 3 were adjusted in order to explore the balance between true and false positives output by the system. At $t_1 = 0.95$, $t_2 = 0.95$, after testing 153,459 images, the system recovered 25/59 of the test set's lenses and returned three false positives. These settings were used as a basis for the wider search. A subset of candidates returned from the test set, as well as those not detected, are depicted in Figure 5. Some of the lenses missed include cluster-scale lenses, red sources and possible edge-on spiral deflectors, which were not simulated in the training set; others are more similar to the simulated lenses.

We applied the same pipeline to 171 square degrees of the CFHTLS survey for which *i*, *r* and *g* band data were available. The results of the search with these parameters are summarised in Table 5. Classifying the images took approximately 100 GPU-days on NVidia K20 GPUs with 2496 cores each. After examining all of the 60x60 postage stamps with both ConvNets, 18,861 candidates were identified by the system, representing 0.1% of the survey area or about one source in 1900. Out of the 59 sources in our test set of real lens candidates, the final candidate set included 22 (37%) of them (three of the lenses found in the test set search were dropped due to minor differences in position in the cutout between the two searches). The candidate set included a total of 63 of 565 previously reported lenses or candidates (11%), and 14 of the 103 confirmed lenses (14%). Of the remaining 18,839 candidates, the authors identified 18,400 as low quality (false positives) and 149 as potential lens candidates with grade > 0. Out of 640 million images examined, this represents a false positive rate of about 1 in 35,000. The 199 true positives represent a purity of only 1% for the estimated completeness of 11-14%.

The sample of novel candidates includes six which we rate as grade ≥ 2. These candidates are included in Figure 6 and Table 6.

4.3   Catalogue-based search

To assess the performance of the catalogue-based search, we assign each known lens/candidate to the closest catalogue sources. Of the SPACEWARPS test set lenses, two were too blue and were excluded by the colour cut leaving a test set of 57 lenses.

For the catalogue-based search, each of the 1.4 million selected sources was evaluated with the ConvNets 1-4. As with the whole-survey search, the score thresholds for each ConvNet can be varied in order to assemble subsets of the tested sources to serve as candidate sets. Each subset can be assigned a true positive rate based on the number of test set lenses recovered, and a false positive rate based on the size of the set and the number of known lenses within it. The distribution of these sets in true positive-false positive space, known in machine learning literature as a receiver operating characteristic curve (ROC - Fawcett 2004), succinctly describes the trade-off between precision and recall inherent in an algorithm, and is presented in Figure 7.

At one extreme, selected for high purity and using the four threshold values of (0, 0.95, 0.95, 0.15) for ConvNets 1-4, a candidate set of only 71 candidates was produced containing 4 of the test set lenses and 10 other known lenses or candidates. In other parts of the space, with low thresholds for all of the networks, candidate sets containing hundreds of thousands of images can be produced. In between these two extremes, with thresholds (0, 0.95, 0.55, 0), a candidate set of 2,465 sources is produced containing 23 of the test set lenses. With a completeness of 40% with respect to the SPACE-WARPS lenses, and a candidate set small enough to inspect in under an hour, this set was chosen as representative of likely practical settings and was examined by eye to evaluate overall candidate quality.

The sample contains 117 of the 565 previously known lenses, including 29/103 confirmed lenses. After visual inspection of the 2,465 candidates we identify a further 266 candidates as possible or probable lenses, including 249 possible, 15 probable and four definite lenses. The candidates with scores ≥ 2 are presented in Figure 6 and Table 6. 12 of the galaxies have photometric redshifts, ranging from 0.42 (CN1) to 1.13 (CN16).

Figure 5 depicts a subset of test set lenses and confirmed lenses recovered in the candidate set, and of those not recovered. There are several example of highly elliptical deflectors (potentially edge-on spirals) and redder sources amongst the missed lenses, which differ from those generated for the training set. There are also several cluster-scale lenses, which were also not included in our simulations. In colour-magnitude space, there is not clear difference between the lenses found and those missed. However, the robot performed slightly better on lenses rated as higher quality by astronomers. Of the 59 SPACEWARPS test set lenses, 30 were of grade less than 2, and 29 were of grade 2 and above. Of the 2+ lenses, our system recovered 14/29 (46%), and of those <2, 9/30 (30%).

5   DISCUSSION

5.1   Training networks on simulated images

From the results presented we conclude that convolutional neural networks trained on synthetic lenses are able to develop detectors for lensing features and identify real lenses in survey image data. Our two training sets were designed to simulate strong lenses with parameters such as brightness and Einstein radius similar to those lenses present in CFHTLS and discovered by the human volunteers of the SPACEWARPS project.

As described in Section 2.3, we also used a test set consisting of the 59 SPACEWARPS lenses to aid in setting some of the search parameters, namely ConvNet score thresholds. As the ConvNets are, by design, optimized to detect objects similar to the training set, our robot will not in general succeed at finding lenses that are, for instance, significantly larger in the sky, are of different colour, have point instead of extended sources (i.e. QSOs) or are not galaxy-scale lenses (i.e. clusters).[10]

Unlike a human, the ConvNets demonstrate little ability to generalise the features they have learned to situations that differ from those presented in the training set on which they were optimised. A human being might spot a lens that has the same shape as other examples but differs in colour (for instance, a red-red lens)

---

[10]   We have created training sets that include cluster-scale lenses and lensed QSOs, with preliminary results that indicate that these different morphologies are also learnable, but do not present that work here.
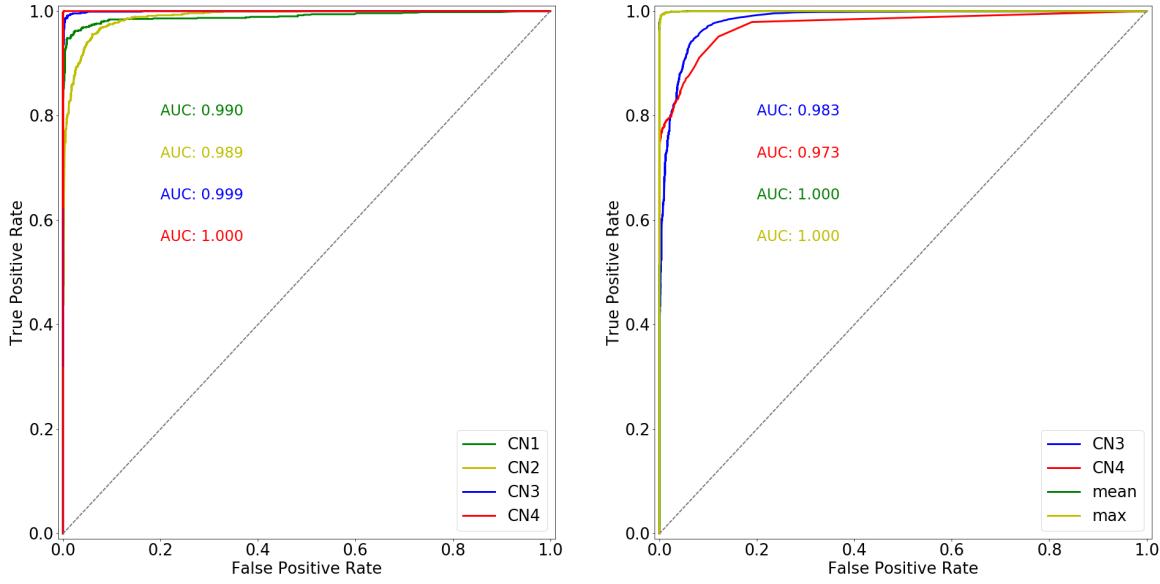
Figure 4. Receiver operating characteristic curves for the trained ConvNets, depicting the trade-off between the true positive rate (recall) on the y axis, and the false positive rate (false positives/all negatives) on the x axis. Each point on the curve represents a threshold setting for the network - a lower threshold identifies more candidates (higher recall) but also more false positives (lower precision).

Table 5. Results of all-survey and catalogue searches.

All-survey search		Catalogue-based search	
Images tested	6.4×10^8	Images tested	1.4×10^6
Detection by either ConvNet	2.0×10^7	Final candidate set	2,465
Detection by both ConvNets	1.6×10^5	Fraction of images returned as candidates	1.8×10^{-3}
Candidates robust under translation	3.5×10^4	Test set lenses/candidates found	23/57 (40%)
Fraction of images returned as candidates	2.9×10^{-5}	Known lenses/candidates found	117/565 (21%)
Final candidate set	18,861	Confirmed lenses found	29/104 (28%)
Test set lenses/candidates found	22/59 (37%)	New lens candidates grade > 0	266
Known lenses/candidates found	63/565 (11%)	New lens candidates grade >= 2	13
Confirmed lenses found	14/104 (13%)	False positives	2097
New candidates	199	Purity	15%
False positives	18,400	Completeness (known lenses)	21-28%
Purity	1%		
Completeness (known lenses)	11-13%		

and decide it is an unusual instance of the class; the ConvNet probably will not, as the convolutional kernels it has developed weight the contributions of the colours according to their prevalence and significance in the training set. Although there is ongoing research into classes of machine learning techniques where this weakness is addressed - for instance, Bayesian Program Learning (Lake et al. 2015), which models visual concepts as simple probabilistic programs - this is an intrinsic feature of ANNs.

A sufficiently complex ANN can be expected to learn more than just the general morphology of a gravitational lens. Any simplifications or unphysicalities in the simulations are likely to be learned by the network. Where an ANN is trained properly, the network's weights will efficiently encode the significant features of the training set. In the case of real-world images, finding such an encoding is a highly complex task, though one at which ANNs have proved highly successful. In the case of simulations, the most efficient such encoding would be the parameters of the simulation code itself; if an ANN is trained on a sufficiently large number of simu-

lated images, it can be expected to become proficient at determining whether an example image could be generated by a given simulator. This type of overfitting to the training set is a hazard of using simulated training data, and so good classifier performance on simulations should be treated with caution. Our own results, where excellent performance on simulated lenses was not replicated on real data, underscores this point.

In this work we deployed ConvNets with relatively simple architectures. Training much deeper networks is feasible. The motivation for deeper, more complex networks is the extraction of a richer feature set from the training data, at the expense of training time, a larger training set, and potential difficulties getting training to converge. Because of the high accuracy on simulated training, validation and test sets, we did not explore deeper networks which we deemed likely to merely overfit further to the simulations. Future work will need to explore whether deeper networks have an impact on the performance on genuine astronomical image data, especially as the simulations improve and become more complex.

Table 6. New potential strong lenses identified in the CFHTLS wide fields by the ConvNet lensfinding robot. The 16 sources consist of the candidates identified by the algorithm that have a quality flag ≥ 2 and are not identified elsewhere in the literature. The i-band magnitude supplied is from CFHTLS Terapix T0007 photometric catlog 3" aperture photmetry. Photometric redshifts for the deflectors are provided where available.

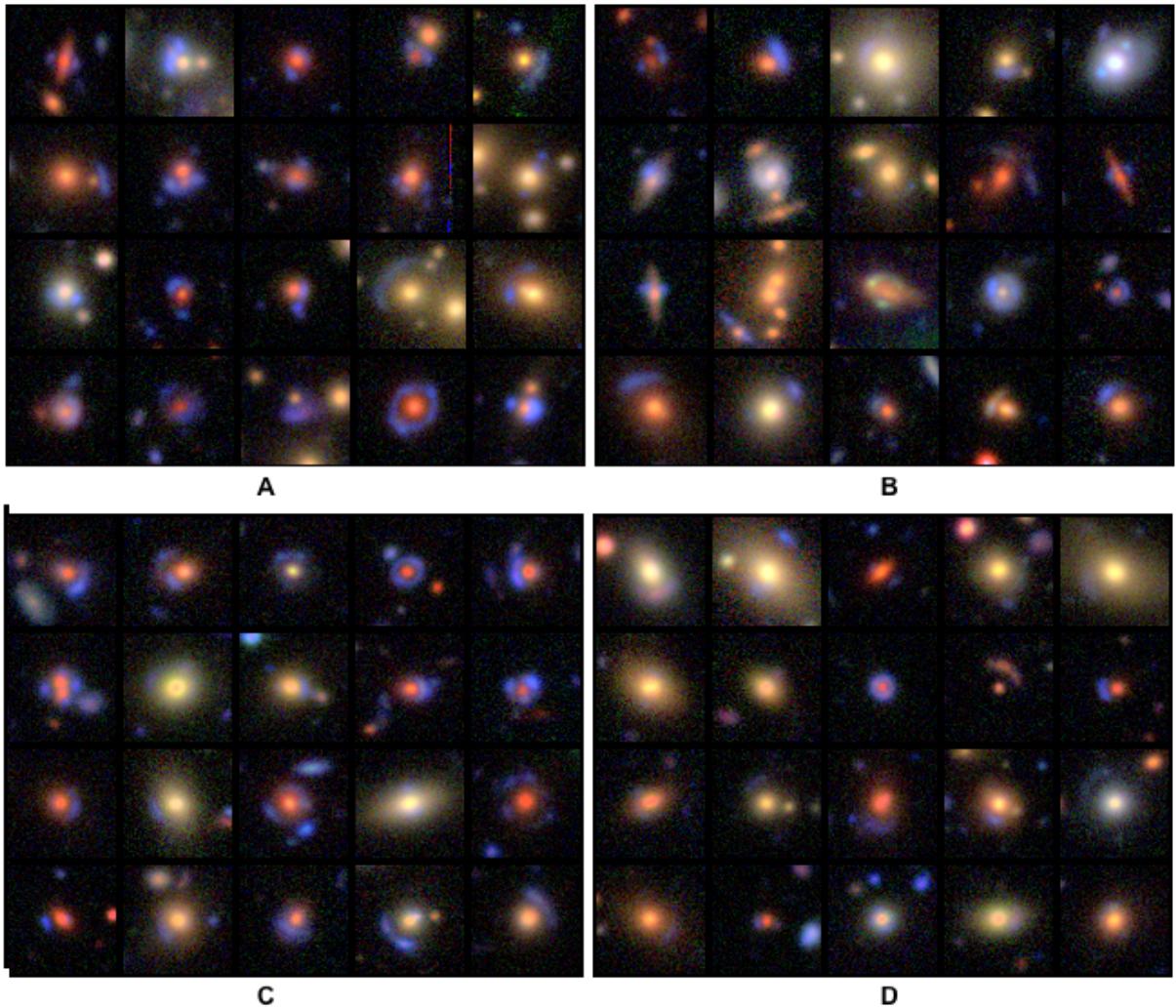| Candidate	search	source	RA	dec	grade	i_{mag}	z_{phot}
CN1	all-survey	1135_114442	32.014397	-6.962067	2.0	19.857	0.42
CN2	all-survey	1134_102957	32.773519	-7.136335	3.0	20.450	0.83
CN3	catalogue	1114_035558	34.866662	-5.488730	2.5	19.18	–
CN4	all-survey	1157_073435	36.528578	-9.983405	3.0	20.323	–
CN5	catalogue	1119_077854	38.123480	-6.227281	2.0	20.67	–
CN6	both	1120_144248	37.142005	-5.996789	2.0	20.68	0.84
CN7	catalogue	1124_121677	33.544766	-6.093784	2.0	21.29	0.79
CN8	catalogue	1133_208513	33.367565	-6.681572	3.0	20.53	0.55
CN9	both	1156_165804	37.090818	-9.645684	2.0	19.74	0.30
CN10	catalogue	1163_117574	31.012133	-9.745038	2.0	21.30	0.87
CN11	catalogue	1203_218233	134.733282	-1.035681	2.0	19.48	–
CN12	catalogue	1309_158230	217.484603	56.535095	2.0	20.27	0.55
CN13	catalogue	1314_020589	210.346656	55.951494	2.0	19.59	–
CN14	both	1328_213514	210.206937	54.738516	2.0	20.47	0.59
CN15	catalogue	1403_048428	330.851737	3.811333	2.0	21.87	–
CN16	catalogue	1424_168469	333.094995	-0.303149	2.0	21.71	1.13

Figure 5. A subset of lenses recovered by the lens finder, and those missed. Top left, A: 20 Lens candidates identified by citizen scientists of the SpaceWarps project (More et al. 2016) recovered by the ConvNet robot in a candidate set of 2465 candidates. Top right, B: 20 SpaceWarps lenses not recovered. Bottom left, C: 20 confirmed lenses recovered in the catalogue-based search. Bottom right, D: 20 confirmed lenses not recovered. The missed SW lenses contain more cluster-scale lenses, redder sources and potential spiral deflectors; the missed confirmed lenses have fainter sources.
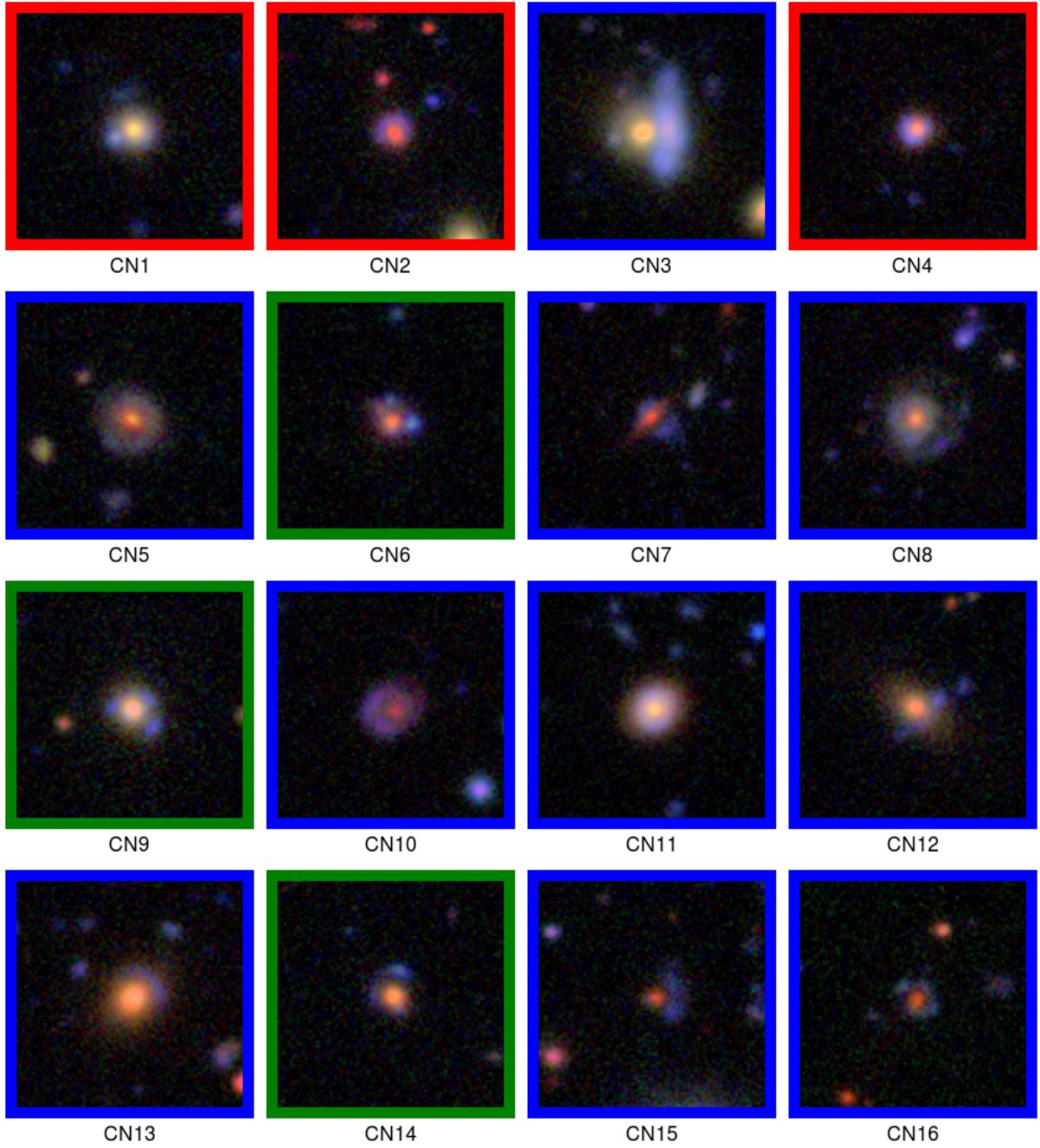
Figure 6. New potential galaxy-galaxy lenses detected by the ConvNet-based lens finder. *gri* composite images are shown, with the border indicating the method of discovery: red = all-survey search, blue = catalogue based, green = both. The sources are described in Table 6.

5.2 Using an ensemble of Neural Networks

The use of ensembles of neural networks in classification or regression problems is a common practice in machine learning (Hansen & Salamon 1990; Zhou et al. 2002). According to the standard procedure, multiple networks are trained using different subsets of the training set and then (for example) averaged together to produce a final score for a given input. In complex computer vision applications this typically provides a small edge over any single network. In the case of the lensfinder, this approach is of little value as the network is already able to classify simulated training, validation and test sets with very high accuracy. The networks' performance drops when generalised to real data.

We used simulated lenses from two different sources to train our networks. Each simulation code took an approach that was physical and realistic but the resulting outputs were slightly different in appearance. By combining the two, we smooth out some of the less realistic features of each simulated set. We find that in the case of our networks, a union of two candidate sets provided good results; we only look at candidates that triggered both networks, ignoring those that were flagged in one network only as likely false positives. Other functions, such as a mean score or max of the two
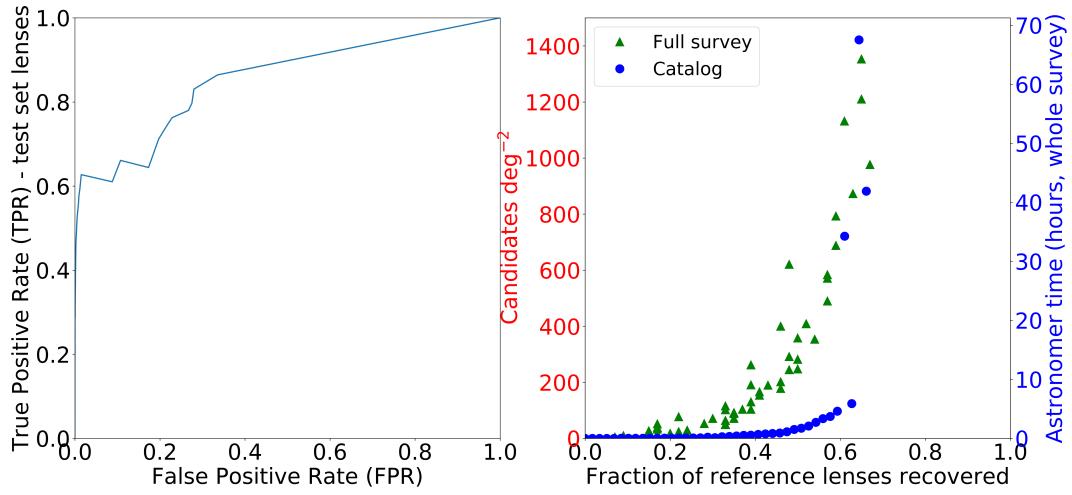
Figure 7. Left: Catalogue-based lensfinder true-positive/false positive response (ROC curve). 20% of the test set can be recovered with a false positive rate of .01%; 40% with a false positive rate of 0.17%; and 60% with a false positive rate of 1.17%. Right: Lensfinder recall vs. time required to inspect the produced candidate set for the whole-survey approach (green triangles) and catalogue-based search (blue circles). For the whole survey, 171 square degrees, we estimate 40% of findable lenses can be recovered with about 15 candidates per square degree to inspect - or one hour of inspection time for the survey.

networks' scores, are also feasible approaches. Although a detailed investigation of the networks' internal activations is complex and beyond the scope of the current work, it appears that the ensemble process is effective as the networks tend to agree most often on a high score where stark lensing features are apparent, but false positives are triggered in different ways.

This approach of constructing multiple simulations and training networks separately may have application in other areas of astronomy where examples are few and simulations are required to build a training set.

We note that combining the two different sets of simulations into one and retraining the network on the combined set did not yield satisfactory results. The combined training set, with an accuracy in training of ~70%, was strictly inferior to either of the separate training sets. There is no theoretical barrier to achieving similar accuracy as the ensemble with a single ConvNet of sufficient complexity, since the logic we employed of developing two sets of feature maps and weighting the outputs could be replicated within the connections of an ANN. Further experimentation with the training sets and the use of a network with additional layers and more artificial neurons is required.

5.3 Catalogue-based versus all-survey search

Searching the entire survey - that is, feeding every pixel of the imaging data through the networks, regardless of the presence of a likely lensing galaxy - has the advantage that the maximum completeness is attainable, since no assumptions are made in selecting a subset of sources to examine. Unusual lenses of high scientific value (complex morphologies, multiple lensed sources, dark matter-dominated deflector) are more likely to be excluded by a catalogue selection, and inaccurate catalogue photometry may exclude others, such as the case where a bright blue source substantially shifts the colour of the foreground galaxy within the photometric aperture used by the catalogue source extractor. The volunteers for the SPACEWARPS CFHTLS blind search were not restricted

to postage stamps of ETGs but shown larger fields containing hundreds of sources, so they were freely able to nominate candidates that differed from the typical morphologies and colours used in training examples.

The disadvantages of such a wide search with automated algorithms are several. Firstly, it is computationally expensive, requiring months of GPU time for a large survey area. Secondly, lower purity in a candidate set can be expected since a much larger number of candidate images are examined (at least two orders of magnitude) per genuine lens, accumulating more false positives. Finally, unless the training set explicitly includes unusual examples (such as a lens with no visible deflector) they are unlikely to be detected in any case by the networks.

Restricting the search for strong lenses to preselected potential deflector galaxies simplifies the search in several ways. Firstly, it reduces the search area enormously, and presents a much purer (though inevitably less complete) set of images to the network. Secondly, a catalogue-based search simplifies the generation of a training set. Both the positive and negative training images can all be centered on a bright elliptical galaxy, since all future candidate images will follow the same convention.

The catalogue-based search was significantly more efficient in recovering known lenses by producing candidate sets of considerably higher purity (precision) for a particular completeness (recall) value as measured against known lenses in the sample. Although the networks trained for the whole-survey search had a lower false positive rate of 1 in 35,000 versus 1 in 671 for the catalogue-based search, this can be explained by the relative ease of distinguishing galaxy-galaxy lenses from empty sky, spiral galaxies, stars and other unlikely candidates.

Of the 63(14) known(confirmed) lens candidates detected in the all-survey search, 44(11) of them were included in the catalogue sample. Of the six novel candidates we rate as grade ≥ 2 in the all-survey search, three of them were also detected in the catalogue-based search.

5.4 Quantifying the performance of the robot

The outputs of the ConvNets are real numbers $\in (0, 1)$ which we interpret as a measure of confidence or of candidate quality. The minimum confidence level for which we include candidates in our output set is a free parameter in this range. Depending on the values chosen, the ConvNets are able to produce a set of candidate images of almost arbitrary size but with highly variable purity and completeness. In practical terms this means that, depending on the particular application, the robot can produce larger or smaller candidate sets by making trade-offs in the purity and completeness.

Analysis of the performance of a lens-finding robot is complicated by several factors. Performance is optimal when it finds all potential lenses (lens grade > 0) and no false positives (grade = 0). Performance degrades both as the number of false positives increases and the fraction of true positives recovered decreases. We can fully populate the confusion matrix, as defined in Table 7, for our system as applied to training, validation and test sets of simulated lenses. Similarly, we can measure performance against the test set of SpaceWarps candidates, since the lens candidates are all known, as presented in Table 8.

It is the robot's performance on real imaging data that is of most interest. On the wider search, quantifying the performance is more complicated, as candidates which are not previously reported as lenses in other searches may not be considered false positives if they are sufficiently interesting. Similarly, we do not know how many lenses remain undetected in the survey and so the false negative rate is likewise uncertain. With this caveat in mind, we use the data from the test set, combined with more approximate metrics gained from the wider search in our consideration of our robot's performance on the CFHTLS sky.

By varying the free parameters t_1 and t_2 (Equation 3) we can more fully explore the balance between precision and recall afforded by our robot. For any point in the (t_1, t_2) space we can plot the rate of true positives (recall) and false positives (False Positives/Condition Negatives) to produce a ROC curve as presented in Figure 4 and Figure 7. The ideal curve includes the point $(x = 0, y = 1)$ where all positive examples are detected with no false positives, and has an area under the curve (AUC) of 1. The worst case case scenario, where the robot guesses randomly, lies on the line $y = x$.

To construct a confusion matrix and estimate purity and completeness (precision and recall) on the real survey imaging data, we use the 565 previously reported lens candidates as an approximation of the complete sample of findable lenses in the survey.

To estimate purity, we also consider interesting novel candidates. Any candidate to which we assign a grade > 0 after visual inspection we consider a true positive; other candidates we count as false positives. Of our final catalogue-based candidate set of 2465 lenses, 117 had been previously identified as potential lenses, including 23/57 (40%) SpaceWarps lenses and 29/103 (28%) confirmed lenses. The authors agreed that 364 candidates were of grade 1 or greater, including 98 of the 117 reported lenses in the sample; 526 images were graded with score > 0 by at least one reviewer, including 102 previously known lenses, meaning that between 379 and 537 of the sample were interesting candidates. Thus when applied to CFHTLS data, our robot produced a sample with a purity of between 15-22%. The 117 of 565 known lenses (22%) returned in our sample, including 28% of confirmed lenses, gives us an estimate of completeness with respect to the highest quality detectable lenses.

Our sample included at most 2086 false positives from a set of

1.4 million true negatives tested, for a false positive rate of 0.15%, or one in 671.

Although we included all the known lenses and candidates previously discovered in CFHTLS image searches in our analysis above, a significant number of them are cluster-scale lenses, have non-elliptical deflectors or red sources, or are extremely faint according to a subjective ranking by the authors. These differ significantly from the examples simulated in the training sets we generated. We estimate approximately 15% of the sample, both confirmed and unconfirmed, meet one or more of these conditions. Excluding these from the known lenses, our lens finder recovered 25% of previously reported and 33% of confirmed lenses; this may better approximate the performance of a robot engineered specifically for lenses of a particular morphological class, i.e. galaxy-galaxy lenses, and give some indication of gains that might be realised with a training set that includes greater morphological diversity.

5.5 Context and practice

The ConvNets were more prone to identify clear false positives than a professional astronomer or even a human volunteer with minimal training; for instance, across the whole survey each ConvNet identified of order 10^7 candidates with confidence > 0.5, amounting to a few percent of images tested. A key challenge was how to best use the classification data to minimise false positives, i.e. candidates we judge very unlikely to be lensing systems. Intrinsic to the lens-finding problem is the rarity of lenses on the sky. If we expect approximately one lens per square degree of sky (as per Treu 2010), then in an all-survey search of the scale we conducted, a false positive rate of only 1 in 1000 would mean that quality lens candidates would be outnumbered by false positives at a ratio of about 4000:1.

An alternate way to examine the trade-off between precision and recall is presented in Figure 7, which plots the fraction of lenses recovered in the candidate set against the average size of the candidate set per square degree of sky. Assuming an astronomer could search these candidates for quality lenses at a rate of 60 per minute[11], the amount of time required to process the whole survey's candidates is indicated on the right. For a whole-survey search, to recover 50% of lenses one would need to examine approximately 250 candidates per square degree, 0.2% of the field's area. To recover a minimum of one high-quality candidate, examining a candidate set of a few hundred postage stamps for the whole survey would be required. The catalogue-based search is more efficient, with 50% recall achievable with only 40 candidates per square degree. By restricting candidate sources even further, to $19.5 < \mathrm{mag}_i < 20.5$ and $1.8 < g - i < 2.5$, and setting the thresholds aggressively we were able to generate small, pure but highly incomplete candidate sets, for instance a set containing only 7 candidates for the entire survey but including 4 known lenses (a purity of 57%). The lensfinder can be used to quickly find some of the best quality lenses, but astronomer time required grows quickly as desired completeness increases (see Section 4.3 and Figure 8).

Table 9 presents estimated astronomer time for recovering galaxy-galaxy lenses from DES and LSST assuming a candidate finder with similar purity and completeness characteristics as the one we applied to CFHTLS. Collett (2015) estimates 1,300 detectable lenses in DES and 62,000 in LSST. Recovering the majority of them from a survey of LSST's size could require months of

---

[11] When presented as 10x10 montages containing 0 to a few quality candidates, we found this rate to be feasible.

	Condition Positive (CP)	Condition Negative (CN)
Test positive	True Positives (TP)	False Positives (FP)
Test negative	False Negatives (FN)	True Negatives (TN)

Table 7. Template for the confusion matrix of a classification algorithm.

	Actual positive	Actual negative
Test positive	25	3
Test negative	34	153,459

Table 8. Confusion matrix for the all-survey test set containing 153,000 images including 59 SpaceWarps lens candidates. The candidate set is produced by taking all candidates where the two ConvNets give a score $s > 0.95$.

Table 9. Estimates of astronomer time required to find 20, 40, 60 and 80% of detectable lenses in the Dark Energy Survey (DES) and Large Synoptic Survey Telescope (LSST) surveys using the ConvNet method assuming similar performance to that presented in this paper. Estimates from Collett (2015) suggest 1300 findable galaxy-galaxy lenses in DES and 62000 in LSST.

Survey	20%	40%	60%	80%
CFHTLS	3 min	30 min	5 hours	4 days
DES	30 min	5 hours	2 days	44 days
LSST	4 hours	3 days	22 days	1.5 years

astronomer time categorising candidates. Although the efficiency of the lensfinder we developed can no doubt be significantly improved upon, these figures highlight the need (and opportunity for) new algorithms that can more efficiently extract the most interesting candidates from the surveys' imaging.

6 CONCLUSIONS

We present an application of convolutional neural networks to the automated identification of potential strong lenses. Deep learning techniques have advanced computer vision in many other fields and have already found many promising applications in astronomy. Our work demonstrates that a ConvNet can extract morphological and colour-space features from examples of strong lenses, and also that the use of simulations in training sets can be used to train a lens-finding robot to be of practical use on real astronomical data. For a survey covering 171 degrees to an r-band depth of ~24.83 we were able to generate a candidate set that was 28% complete in terms of confirmed, findable lenses; 15% pure with respect to possible lenses; and at ~14 candidates per square degree, could be visually inspected by a human in under an hour. The ConvNet-based method allows for higher completeness at the cost of decreasing purity.

Using the pipeline developed here we find that a ConvNet-based lensfinder, under the conditions of the CFHTLS and using a catalogue-based search with optimised settings, could produce a candidate set that yielded of order one good quality lens candidate per square degree of survey sky with an investment of astronomer inspection time of under half a minute each. We are optimistic that this rate of discovery can be replicated or exceeded in other extant and future image surveys.

The rate of discovery achieved with the ConvNets compares favourably to previous robotic searches. Our lensfinder proved more efficient than More et al.'s (2012) CFHTLS lens search using ARCFINDER, which required visual inspection of ~150,000 candidates for a final sample of 127 quality candidates, and is on par with RINGFINDER (Gavazzi et al. 2014), where the algorithm returned 0.4% of sources examined, for a sample size of 2500 candidates. Gavazzi et al estimate 40% completeness based on simulations and follow up of a sub-sample of candidates; our catalogue-based search returned 0.2% of ETGs examined and we place a

lower bound on completeness of 28%. The analysis presented in Section 5.4 suggests that at current performance, a completeness of 40% of findable lenses is achievable with a candidate set of ~8000 candidates, requiring about three hours per astronomer to sift. We expect that with more realistic training sets and different ensemble strategies this performance can be significantly improved upon.

CFHTLS was chosen as a yardstick to evaluate ConvNet performance as it has been extensively searched for lenses using other methodologies. Given the performance we obtained, this method would appear to be a promising way to explore new fields. Using synthetic training sets generated with parameters matching other current and upcoming surveys such as DES and LSST, the convents can be retrained and readily applied to another data pipeline. As well as generating candidate sets from these surveys, this method could also be used to produce candidates for revision by citizen scientists, complementing efforts like SpaceWarps by screening candidates but relying on human volunteers and the SpaceWarps quality algorithm to purify the sample before review by astronomers.

Given the demonstrated effectiveness of convolutional neural networks in computer vision applications such as classification and detection of everyday objects, it has proven to be a safe assumption that, if there is enough information in an image for a human expert to extract meaning, a properly-designed ConvNet is likely to also converge on a suitable feature extraction strategy. The SpaceWarps project, by providing rapid training to human volunteers, demonstrated that enough information is present in images of galaxies under the conditions of CFHTLS resolution and seeing.

The need for simulated lenses to train Convolutional Neural Networks is potentially a limiting factor in their utility in practice, as they can only ever be as good as the simulations are realistic. Our results underscore the risk that Convolutional Neural Networks trained on simulations may learn to overfit to the peculiarities of the simulation code, and that good performance on a simulated training and test set will not, as a rule, translate directly to the real universe. Reports of good performance measured in simulations only should therefore be treated with caution, as it may merely indicate that the network has learned to spot a subtle bias or artifact present in simulated lenses rather than physical lensing features.

Futher work includes refining the training sets to reduce false positives and to better detect lenses with a wider range of morphologies, including lensed QSOs and cluster-scale lenses; testing an increase in the size of the training sets and the number of convolutional layers in the network; and retraining the networks with good candidates and false positives identified in visual inspection. Exploring the ensemble approach further, for instance with training sets composed of simulated lenses in discrete bins of source magnification and Einstein radius, may aid in developing a detector capable of discriminating the brightest and most promising lenses more efficiently.

Convolutional neural networks have also recently been employed for lens finding in the Kilo-Degree Survey (KiDS) (Petrillo et al. 2017) and simulations of LSST (Lanusse et al. 2017). The dif-
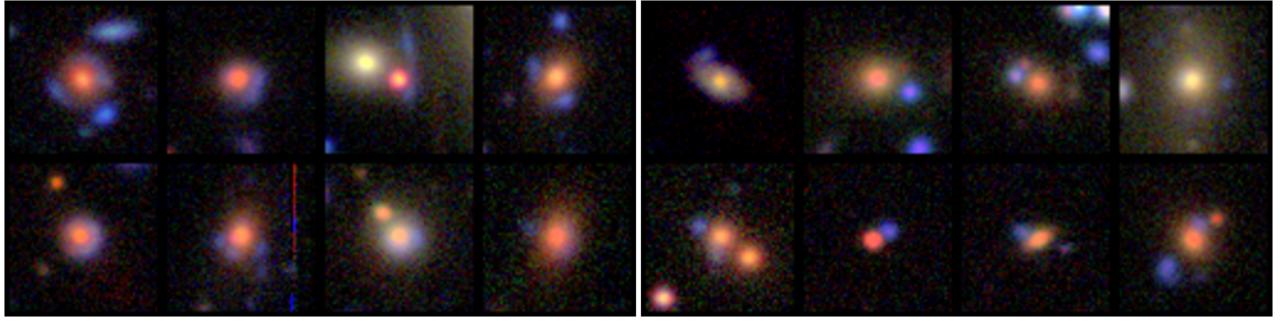
Figure 8. An example of a candidate set with high purity (50%) but low completeness (1.4%). By restricting the search to sources with $19.5 < \text{mag}_i < 20.5$ and $1.8 < g - i < 2.5$, and setting the ConvNet thresholds such that only a small candidate set is returned, we produced this set of 16 candidates including eight previously known lenses (left).

ferences in survey data quality and the types of lens targeted make a direct comparison difficult. However, our method of using multiple training sets and ConvNets appears to give more probable lens candidates per square degree than the Petrillo et al ConvNets, although at the cost of a factor four more human classification time. This lower purity is unlikely to be a relative deficiency of our method; we targeted smaller Einstein radius lenses where seeing makes the classification problem much harder.

References

Alard C., 2006, arXiv:astro-ph/0606757
Amiaux J., et al., 2012, arXiv:1209.2228 [astro-ph] 10.1117/12.926513, p. 84420Z
Auger M. W., Treu T., Bolton A. S., Gavazzi R., Koopmans L. V. E., Marshall P. J., Moustakas L. A., S. Burles 2010, ApJ, 724, 511
Blandford R. D., Narayan R., 1992, ARA&A, 30, 311
Bom C. R., Makler M., Albuquerque M. P., Brandt C. H., 2017, A&A, 597, A135
Bonvin V., et al., 2016, MNRAS, p. stw3006
Bottou L., 2010, in Lechevallier Y., Saporta G., eds, , Proceedings of COMPSTAT'2010. Physica-Verlag HD, pp 177–186, doi:10.1007/978-3-7908-2604-3_16
Bradač M., Schneider P., Steinmetz M., Lombardi M., King L. J., Porcas R., 2002, A&A, 388, 373
Brault F., Gavazzi R., 2015, A&A, 577, A85
Cabanac R. A., et al., 2007, A&A, 461, 813
Cao Z., Qin T., Liu T.-Y., Tsai M.-F., Li H., 2007, in Proceedings of the 24th International Conference on Machine Learning. ICML '07. ACM, New York, NY, USA, pp 129–136, doi:10.1145/1273496.1273513
Chan J. H. H., Suyu S. H., Chiueh T., More A., Marshall P. J., Coupon J., Oguri M., Price P., 2015, ApJ, 807
Choi Y.-Y., Park C., Vogeley M. S., 2007, ApJ, 658, 884
Collett T. E., 2015, ApJ, 811, 20
Collett T. E., Auger M. W., 2014, MNRAS, 443, 969
Collett T. E., et al., 2017, arXiv:1703.08410 [astro-ph]
Connolly A. J., et al., 2010, in Proc. SPIE. pp 77381O–77381O–10, doi:10.1117/12.857819
Dieleman S., Willett K. W., Dambre J., 2015, MNRAS, 450, 1441
Duchi J., Hazan E., Singer Y., 2011, J. Mach. Learn. Res., 12, 2121
Einstein A., 1936, Science, 84, 506
Elyiv A., Melnyk O., Finet F., Pospieszalska-Surdej A., Chiappetti L., Pierre M., Sadibekova T., Surdej J., 2013, MNRAS, 434, 3305
Estrada J., et al., 2007, ApJ, 660, 1176
Fawcett T., 2004, Mach. Learn., 31, 1
Fukushima K., 1980, Biol. Cybernetics, 36, 193
Gavazzi R., Marshall P. J., Treu T., Sonnenfeld A., 2014, ApJ, 785, 144

Glorot X., Bengio Y., 2010, in International Conference on Artificial Intelligence and Statistics. pp 249–256
Goodfellow I., Pouget-Abadie J., Mirza M., Xu B., Warde-Farley D., Ozair S., Courville A., Bengio Y., 2014, in Ghahramani Z., Welling M., Cortes C., Lawrence N. D., Weinberger K. Q., eds, , Advances in Neural Information Processing Systems 27. Curran Associates, Inc., pp 2672–2680
Hansen L. K., Salamon P., 1990, IEEE Trans. Pattern Anal. Mach. Intell., 12, 993
He K., Zhang X., Ren S., Sun J., 2015, ArXiv Prepr. ArXiv151203385
Hecht-Nielsen R., 1989, in , International Joint Conference on Neural Networks, 1989. IJCNN. pp 593–605 vol.1, doi:10.1109/IJCNN.1989.118638
Hinton G. E., Salakhutdinov R. R., 2006, Science, 313, 504
Hinton G. E., Srivastava N., Krizhevsky A., Sutskever I., Salakhutdinov R. R., 2012, arXiv:1207.0580 [cs]
Hoyle B., 2016, Astron. Comput., 16, 34
Huertas-Company M., et al., 2015, ApJS, 221, 8
Hyde J. B., Bernardi M., 2009, MNRAS, 396, 1171
Ivezic Z., et al., 2008, arXiv:0805.2366 [astro-ph]
Jia Y., Shelhamer E., Donahue J., Karayev S., Long J., Girshick R., Guadarrama S., Darrell T., 2014, arXiv:1408.5093 [cs]
Jordan M., Mitchell T., 2015, Science, p. 255
Joseph R., et al., 2014, A&A, 566, A63
Keeton C. R., 2001, arXiv:astro-ph/0102340
Krizhevsky A., Sutskever I., Hinton G. E., 2012, in Pereira F., Burges C. J. C., Bottou L., Weinberger K. Q., eds, , Advances in Neural Information Processing Systems 25. Curran Associates, Inc., pp 1097–1105
Lake B. M., Salakhutdinov R., Tenenbaum J. B., 2015, Science, 350, 1332
Lanusse F., Ma Q., Li N., Collett T. E., Li C.-L., Ravanbakhsh S., Mandelbaum R., Poczos B., 2017, preprint, 1703, arXiv:1703.02642
LeCun Y., Boser B., Denker J. S., Henderson D., Howard R. E., Hubbard W., Jackel L. D., 1989, Neural Comput., 1, 541
Lecun Y., Bottou L., Bengio Y., Haffner P., 1998, Proc. IEEE, 86, 2278
Lenzen F., Schindler S., Scherzer O., 2004, A&A, 416, 11
Marshall P. J., Hogg D. W., Moustakas L. A., Fassnacht C. D., Bradač M., Tim Schrabback Blandford R. D., 2009, ApJ, 694, 924
Marshall P., Sandford C., More A., More B., More H., 2015, Astrophysics Source Code Library, p. ascl:1511.014
Marshall P. J., et al., 2016, MNRAS, 455
More A., Cabanac R., More S., Alard C., Limousin M., Kneib J.-P., Gavazzi R., Motta V., 2012, ApJ, 749, 38
More A., et al., 2016, MNRAS, 455
Nair V., Hinton G. E., 2010, in Proceedings of the 27th International Conference on Machine Learning (ICML-10). pp 807–814
Newton E. R., Marshall P. J., Treu T., Auger M. W., Gavazzi R., Bolton A. S., Koopmans L. V. E., Moustakas L. A., 2011, ApJ, 734
Oguri M., Marshall P. J., 2010, MNRAS, 405, 2579
Oguri M., et al., 2012, AJ, 143, 120
Oguri M., Rusu C. E., Falco E. E., 2014, MNRAS, 439

Ostrovski F., et al., 2017, MNRAS, 465

Petrillo C. E., et al., 2017, arXiv:1702.07675 [astro-ph]

Quider A. M., Pettini M., Shapley A. E., Steidel C. C., 2009, MNRAS, 398

Refsdal S., 1964, MNRAS, 128, 307

Rosenblatt F., 1957, Cornell Aeronaut. Lab

Russakovsky O., et al., 2015, Int J Comput Vis, 115, 211

Schawinski K., Zhang C., Zhang H., Fowler L., Santhanam G. K., 2017, arXiv:1702.00403 [astro-ph, stat]

Schneider P., Kochanek C., Wambsganss J., 2006, Gravitational Lensing: Strong, Weak and Micro. Saas-Fee Advanced Courses Vol. 33, Springer Berlin Heidelberg, Berlin, Heidelberg, doi:10.1007/978-3-540-30310-7

Seidel G., Bartelmann M., 2007, A&A, 472, 12

Simonyan K., Zisserman A., 2014, arXiv:1409.1556 [cs]

Sonnenfeld A., Treu T., Gavazzi R., Suyu S. H., Marshall P. J., Auger M. W., Nipoti C., 2013, ApJ, 777, 98

Sonnenfeld A., Treu T., Marshall P. J., Suyu S. H., Gavazzi R., Auger M. W., Nipoti C., 2015, ApJ, 800

Suyu S. H., et al., 2013, ApJ, 766

Sygnet J. F., Tu H., Fort B., Gavazzi R., 2010, A&A, 517, A25

Szegedy C., Reed S., Erhan D., Anguelov D., 2014, ArXiv Prepr. ArXiv14121441

Tewes M., et al., 2013, A&A, 556

Thanjavur K. G., 2009, PhD Thesis. University of Victoria, Canada

The DES Collaboration 2005, arXiv:astro-ph/0510346

Treu T., 2010, ARA&A, 48, 87

Treu T., Ellis R. S., 2015, Contemp. Phys., 56, 17

Treu T., Koopmans L. V. E., 2002, ApJ, 575, 87

Treu T., Koopmans L. V. E., 2004, ApJ, 611, 739

Walsh D., Carswell R. F., Weymann R. J., 1979, Nature, 279, 381

Wambsganss J., 1998, Living Reviews in Relativity, 1, 12

Zeiler M. D., 2012, arXiv:1212.5701 [cs]

Zeiler M. D., Fergus R., 2014, in Fleet D., Pajdla T., Schiele B., Tuytelaars T., eds, , Vol. 8689, Computer Vision – ECCV 2014. Springer International Publishing, Cham, pp 818–833

Zheng W., et al., 2012, Nature, 489, 406

Zhou Z.-H., Wu J., Tang W., 2002, Artificial Intelligence, 137, 239

Zwicky F., 1937, Phys. Rev., 51, 290